Research Article

Xiaofang Sun, Meng Wang, Guicai Li*, and Yuanyuan Wang

Regional-scale drought monitor using synthesized index based on remote sensing in northeast China

https://doi.org/10.1515/geo-2020-0037
received May 20, 2019; accepted December 18, 2019

Abstract: Drought has a significant impact on agricultural, ecological, and socioeconomic spheres. Although many drought indices have been proposed until now, the detection of droughts at regional scales still needs to be further studied. The Standardized Vegetation Index (SVI) that represents vegetation growing condition, the Standardized Water Index (SWI) that represents canopy water content, and the Evaporative Stress Index (ESI) that quantifies anomalies in the ratio of actual to potential evapotranspiration were calculated based on the Moderate-resolution Imaging Spectroradiometer (MODIS) data. A new remote sensing-based Vegetation Drought Monitor Synthesized Index (VDSI) was proposed by integrating the SVI, SWI, and ESI in the northeast China. When tested against the *in situ* Standardized Precipitation Evapotranspiration Index (SPEI), VDSI with proper weights of three variables outperformed individual remote sensing drought indices. The county-level yields of the main crops in the study area from 2001 to 2010 were also used to validate the VDSI. The correlation analysis between the yield data and the VDSI data during the crop growing season was performed, and its results showed that VDSI during the crop reproductive growth period was strongly correlated with the variation of crop yield. It was proved that this index is a potential indicator for assessment of the spatial pattern of drought severity in northeast China.

Keywords: vegetation drought monitor synthesized index (VDSI), crop yields, Northeast China

1 Introduction

Drought is a major disaster, and it causes huge harm to agriculture, society, economy, and environment. As the world's most damaging and pressing natural disaster, drought collectively affects more people than any other devastating climate-related hazards [1]. There are various types of droughts such as agricultural, meteorological, hydrological, and socioeconomic droughts [2]. In essence, agricultural drought refers to soil moisture deficiency that leads to a decrease in the crop yield. Meteorological drought is defined as rainfall deficiency. Hydrological drought refers to low water availability. Socioeconomic drought causes damage to the economy and human life [3]. The huge economic losses and social impacts in China have been created by the agricultural drought. According to statistics, 70–80 million tons of food is lost in China each year due to drought, which accounts for 17% of the total yield [4]. Northeast China is one of the main producing regions of commercial crops (maize and rice) and economic crop (soybean) in China. It accounted for nearly 50% of the national soybean production [5]. Northeast China often suffers drought since it is adjacent to the semiarid region of northern China and the Mongolian Plateau [6]. In recent years, droughts were notable both in severity and in extent over some parts of this region [7]. Therefore, it is essential to quantify the drought accurately to mitigate its adverse effects on the agriculture and the economy.

Many drought indices have been developed and used in different contexts for drought monitoring. Some prominent climate-based drought indices such as the Palmer Drought Severity Index (PDSI), the Standardized Precipitation Index (SPI), and the Standardized Precipitation Evapotranspiration Index (SPEI) are widely used [8]. The

* **Corresponding author: Guicai Li,** National Satellite Meteorological Center, China Meteorological Administration, Beijing, 100081, China, e-mail: ligc@cma.gov.cn
Xiaofang Sun, Meng Wang: School of Geography and Tourism, Qufu Normal University, Rizhao, 276800, China
Yuanyuan Wang: National Satellite Meteorological Center, China Meteorological Administration, Beijing, 100081, China

main constraint for the operational use of PDSI and SPEI is their local character. They are calculated from the point-based weather data collected at the meteorological stations, which are the most accurate data. However, weather datasets are not available in between stations. Interpolation methods such as inverse distance weighted (IDW), kriging, or high accuracy surface modeling (HASM) must be used to estimate the values of the drought indices between weather stations and to obtain a continuous spatial coverage of data. Spatial interpolation often leads to uncertainties [9]. In regions where the weather stations are distributed sparsely, the spatial accuracy and detail in the drought patterns are further decreased.

Remote sensing data are more suitable for spatially continuous drought monitoring in large geographic areas. A series of drought indices calculated based on the remote sensing data have been used to detect regional drought events in different regions around the world [10–15]. Among the various remote sensing-based drought indices, the Normalized Difference Vegetation Index (NDVI) derived from reflectance radiated in the near-infrared and visible red wavebands has been most widely used for drought monitoring. A series of other indices reflecting vegetation conditions were developed based on NDVI, such as the Vegetation Condition Index (VCI) and the Standardized Vegetation Index (SVI) [16,17]. They are extracted from red and near-infrared channels. Similarly, the Temperature Condition Index (TCI) is an example of thermal drought index, which is calculated based on the maximal and minimal brightness [16]. Compared with the aforementioned indices, the Normalized Difference Water Index (NDWI) is more sensitive to vegetation water content [18]. It is calculated from shortwave infrared (SWIR) and near-infrared channels. The Evaporative Stress Index (ESI) was defined and evaluated by Anderson et al. [19]. It represents temporal anomalies in the ratio of actual evapotranspiration (ET) to potential ET. ESI performs similar to precipitation-based indices, but can be produced at a high spatial resolution without requiring any in situ rainfall data [19].

Furthermore, some studies found that the synthesis of several single drought indices could monitor drought more accurately [20]. The Vegetation Health Index (VHI) based on the additive combination of VCI and TCI is a typical example of this category. Compared with VCI or TCI alone, VHI was proved to be more accurate in drought monitoring [10,21]. Rhee et al. proposed the Scaled Drought Condition Index (SDCI), which was calculated based on the remote sensing data [22]. It combines the land surface temperature (LST) and NDVI data from Moderate Resolution Imaging Spectroradiometer (MODIS) and precipitation data from Tropical Rainfall Measuring Mission (TRMM). Each variable is combined with the selected weight. When tested against PDSI, SPI, and Z-Index, SDCI performed better than existing indices such as NDVI in different climate divisions. The Microwave Integrated Drought Index (MIDI) was developed to monitor short-term meteorological drought distribution in North China by integrating three variables: TRMM-derived precipitation, Advanced Microwave Scanning Radiometer for Earth observing System (AMSR-E)-derived soil moisture, and AMSR-E-derived LST. MIDI with proper weight for three components outperformed individual remote sensing drought indices in monitoring drought [23]. The Synthesized Drought Index (SDI) defined as a principal component of VCI and TCI from MODIS, and Precipitation Condition Index (PCI) from TRMM, has been used to monitor comprehensive drought in Shandong province of China [13]. Hao et al. proposed the Optimized Meteorological Drought Index (OMDI) and the Optimized Vegetation Drought Index (OVDI) from multi-source satellite data to monitor drought in Southwest China [24]. In addition to the indices solely using the satellite data, there are also synthesized indices that combine the remote sensing data with the *in situ* data, such as the Vegetation Drought Response Index (VegDRI) [25]. It is useful in areas with dense *in situ* data.

This study seeks to identify a vegetation drought monitor-synthesized index based on the remote sensing data that can be used for vegetation drought monitoring in northeast China. We proposed a combination of three remote sensing variables, a vegetation growing condition component using SVI derived from NDVI, a vegetation water content component using the Standardized Water Index (SWI) derived from NDWI, and an evaporative component using ESI quantifies anomalies in the ratio of actual to potential evapotranspiration. The Nadir Bidirectional Reflectance Distribution Function (BRDF)–Adjusted Reflectance (NBAR) data were applied. This process has removed the variability caused by angular effects and thus has been reported to improve the accuracy of surface variability detection [26]. The *in situ* SPEI and crop yields were used to assess the applicability and the reliability of the drought index proposed.

2 Study area and data sources

2.1 Study area

This study was carried out in the northeastern part of China, with longitude ranging from E 118°53′ to E 135°05′ and latitude ranging from N 38°43′ to N 53°34′ (Figure 1).

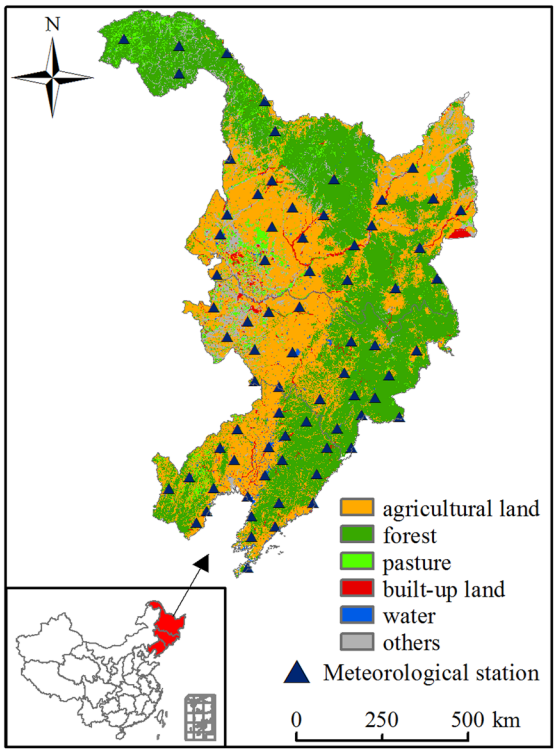

Figure 1: Distribution of the meteorological stations and land cover map of the study area.

This area consists of three provinces: Heilongjiang, Jilin, and Liaoning. Its total area is about $79.18 \times 10^4\,km^2$, including $26.44 \times 10^4\,km^2$ of agricultural lands (33.39%) [27]. Agriculture in this area is strongly dependent on rainfall, and therefore, this area is easily influenced by drought. The ratios of irrigated and rainfed croplands are 32% and 68%, respectively. The region has a temperate continental monsoon climate with a mean summer temperature of 20–25°C and annual rainfall of approximately 500–800 mm. July, August, and September receive the maximum rainfall. The spring months have low rainfall and dry character in general. The study area is an important agricultural region in China, and the dominant crops are soybean, maize, rice, and spring wheat. The growing season for these crops is from late April to late September. The agriculture is frequently affected by climate-related disasters such as drought and snow hazard.

2.2 *In situ* meteorological data

The monthly mean temperature data and total monthly precipitation data were obtained from China Meteorological Data Sharing Service System of China Meteorological Administration (http://cdc.cma.gov.cn/). In the study area, a total of 95 weather stations are available (Figure 1). SPEI was calculated using R program based on the meteorological data from these 95 weather stations.

2.3 Remote sensing data

MODIS data products were used to calculate drought indices. They were downloaded from the website https://search.earthdata.nasa.gov/. The study area is covered by six MODIS path/row tiles (h25v03, h25v04, h26v03, h26v04, h27v04, and h27v05). These tiles were mosaicked and reprojected from a sinusoidal to an Albers Conical Equal Area projection, using a bilinear re-sample operator in MODIS re-projection tool (MRT) from the website (https://lpdaac.usgs.gov/tools).

The MODIS NBAR data product (MCD43A4) was used to calculate the vegetation indices. MODIS NBAR data are produced every 16 days with a spatial resolution of 1 km. The MCD43A4 product uses multiangle surface reflectance values to model the data that would have been obtained from a nadir view and the mean solar zenith angle of the 16-day compositing period [28,29]. The NBAR dataset is produced every 8 days using the combined data from MODIS instruments on the Aqua and Terra satellites. In this study, monthly reflectance data were produced using the maximum value composite (MVC) method based on the 8-day NBAR dataset. For a given pixel, the MVC algorithm selects reflectance corresponding to the highest value among the 8-day data belonging to each month.

The MODIS evapotranspiration (ET) and potential evapotranspiration (PET) products (MOD16A2) at 1 km resolution and 8-day composite temporal resolution from 2001 to 2010 were downloaded from the NASA Internet data portal mentioned earlier. Monthly average values of ET/PET were calculated with the number of days belonging to each month based on the 8-day ET/PET provided metadata after masking the filled and missing values [18]. The process was finished in the interactive data language/environment for visualizing images (IDL/ENVI) software environment. The MOD16 ET/PET algorithm uses the well-known Penman–Monteith equation to calculate ET and integrates both P–M and Priestley–Taylor methods to estimate PET [30].

2.4 Crop yield data

The soybean and maize yield data of each county in Northeast China from 2001 to 2010 were obtained from the

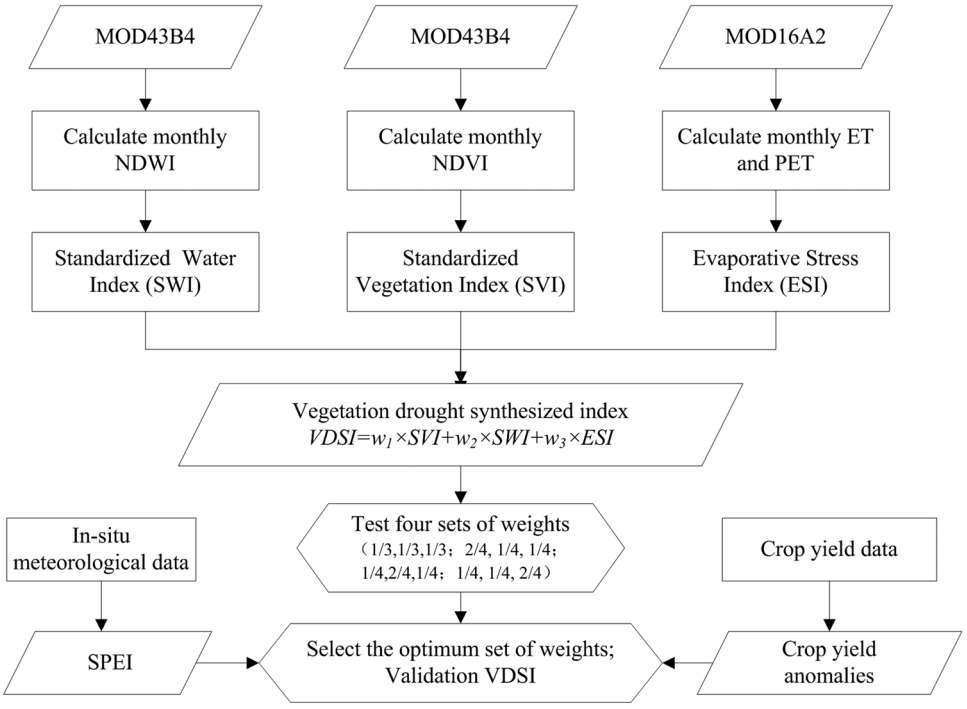

Figure 2: Methodological flowchart.

Agricultural Yearbook of the three provinces, which were published annually by China Agriculture Press in Beijing. The unpublished data were obtained from county level bureaus. A preliminary quality check was conducted. Observations were flagged as outliers when they fell outside the range of biophysically attainable yield records [31].

2.5 Land use data

Land use maps of the study area for 2005 were produced by the Chinese Academy of Sciences through human–machine interactive interpretation based on the Landsat Thematic Mapper (TM) data [32]. The original land use classes derived from these land use maps were classified into 25 land use categories. We aggregated the original land cover type into six main classes (Figure 1).

3 Methodology

This research aimed to integrate multisource vegetation response information for drought monitoring. First, the SVI that reflects the vegetation growing condition, the SWI that reflects the canopy water content, and the Evaporative Stress Index (ESI) that quantifies anomalies in the ratio of actual to potential evapotranspiration were calculated using the surface reflectance data and the ET/PET data. Then, the additive combinations of SVI, SWI, and ESI were produced, and four sets of weights were tested. Finally, *in situ* SPEI and the yearly crop yield data were used to validate the combined index. The research flowchart is shown in Figure 2.

3.1 Computation of drought indices

3.1.1 Standardized vegetation index

To calculate SVI, NDVI was calculated first and is formulated as follows

$$\mathrm{NDVI} = \frac{\rho_{\mathrm{band2}} - \rho_{\mathrm{band1}}}{\rho_{\mathrm{band2}} + \rho_{\mathrm{band1}}} \quad (1)$$

where ρ_{band1} and ρ_{band2} are NBAR red and near-infrared bands, respectively.

SVI was derived based on the calculation of Z scores, a deviation of the NDVI mean in unites of standard deviation over a time series. The SVI is formulated as follows:

$$\mathrm{SVI} = \frac{\mathrm{NDVI} - \mathrm{NDVI}_{\mathrm{mean}}}{\mathrm{NDVI}_{\sigma}} \quad (2)$$

where the $NDVI_{mean}$ defines the normal field, averaged over all years studied, and the denominator ($NDVI_{\sigma}$) is the standard deviation.

3.1.2 Standardized water index

The SWI was calculated on the basis of the Normalized Difference Water Index (NDWI). NDWI is a satellite-derived index from the NIR and SWIR channels that reflect changes in both the water content (absorption of SWIR radiation) and the spongy mesophyll in vegetation canopies. It is defined by the following equation:

$$\mathrm{NDWI} = \frac{\rho_{\mathrm{band2}} - \rho_{\mathrm{band5}}}{\rho_{\mathrm{band2}} + \rho_{\mathrm{band5}}} \tag{3}$$

where ρ_{band2} and ρ_{band5} are the NBAR reflectance value at 857 nm and 2,130 nm, respectively. Therefore, the NDWI is sensitive to vegetation water content. SWI is based on the calculation of Z score of NDWI, which is a deviation from the mean in unite of standard deviation. Thus, the SWI is expressed as follows:

$$\mathrm{SWI} = \frac{\mathrm{NDWI} - \mathrm{NDWI}_{\mathrm{mean}}}{\mathrm{NDWI}_{\sigma}} \tag{4}$$

where the $NDWI_{mean}$ defines the normal field, averaged over all years studied, and the denominator ($NDWI_{\sigma}$) is the standard deviation.

3.1.3 Evaporative stress index

The ESI that quantifies anomalies in the ratio of ET to PET is calculated by the following equations:

$$f = \frac{\mathrm{ET}}{\mathrm{PET}} \tag{5}$$

$$\mathrm{ESI} = \frac{f - f_{\mathrm{mean}}}{f_{\sigma}} \tag{6}$$

where ET and PET are from MOD16A2 dataset [33]. f_{mean} defines the normal field, averaged over all years studied, and the denominator (f_{σ}) is the standard deviation.

3.2 The synthesized index construction method

We proposed a new drought index, the Vegetation Drought Synthesized Index (VDSI), which is the additive combination of the SVI, SWI, and ESI:

Table 1: The weight sets used in this study

	w_1	w_2	w_3
SI-1	1/3	1/3	1/3
SI-2	2/4	1/4	1/4
SI-3	1/4	2/4	1/4
SI-4	1/4	1/4	2/4

SI, synthesized index.

$$\mathrm{VDSI} = w_1 \times \mathrm{SVI} + w_2 \times \mathrm{SWI} + w_3 \times \mathrm{ESI} \tag{7}$$

where w_1, w_2, and w_3 are the weights for SVI, SWI, and ESI, respectively. The contribution of each component to drought processes is difficult to be evaluated because of the lack of data. Therefore, some similar studies assumed the weights to be equal [34,35]. In this research, four sets of weights were tested (Table 1). The correlations between SPEI and SIs (SI-1, SI-2, SI-3, and SI-4) were used to select the optimum weights set. The SI that showed the highest correlation to SPEI was selected as the optimum drought index and was defined as the Vegetation Drought Synthesized Index (VDSI).

3.3 Validation

The SPEI was computed based on the monthly precipitation and air temperature data at 95 stations over Northeast China from 2001 to 2010. SPEI is a widely used drought index [36], which has been accepted for research because of its well-known advantages: the SPEI combines the sensitivity of PDSI to changes in ET demand with the multi-temporal characteristic of the SPI. One-month, 3-month, 6-month, 9-month, and yearly SPEI values (SPEI-1, SPEI-3, SPEI-6, SPEI-9, and SPEI-12) were calculated using *in situ* precipitation and temperature data to select the best data source to derive the optimal SIs. The remote sensing-based synthesized indices were extracted at the location of the meteorological stations, and correlation analyses were performed between the synthesized indices and the *in situ* reference data SPEI.

Crop yield statistics of 10 years (i.e., 2001–2010) at the county level were used to validate synthesized drought index. Several factors may lead to fluctuation of crop yield, such as nutrient status, diseases, chilling damage, and insects; however, drought disaster is one of the main factors that lead to the crop yield decrease. Soybean and maize are the two main crops of northeast China. Therefore, the yields of soybean and maize were

used to test VDSI in the growing period. In this region, the fertility of the cropland in each county is different, and the productivity of crops increases gradually from year to year due to the improvement in the agricultural technology. Henceforth, the crop yield anomaly was used for comparison with drought indices. The crop yield anomaly is calculated as follows:

$$\mathrm{St\_}Y = \frac{Y_i - \bar{Y}}{Y_\sigma} \tag{8}$$

where St_Y is the standardized variable of crop yield, Y_i is the crop yield in I year of one county, $\bar{Y}$ is the average from 2001 to 2010, and Y_σ is the standard deviation of crop yield during 2000–2010.

Correlation analyses between VDSI values of each month in the crop growing season and yearly crop yield anomaly were performed. Counties with the agriculture land less than 30% of the total area were excluded from the analysis. For the counties with the agriculture land larger than 30% of the total area, the mean VDSI values of pixels within the agriculture land for each county were correlated with the county level crop yield anomaly data.

4 Results and discussion

4.1 Comparison of remote sensing drought indices with SPEI

The remote sensing-based synthesized indices were extracted at the point location of the meteorological stations, and the Pearson correlation coefficients were calculated between the remote sensing-based index values and the *in situ* 1-, 3-, 6-, 9-, and 12-month SPEI values. The correlations varied among the different indices and time scales (Table 2).

Table 2: Correlation coefficient values between remote sensing variables and *in situ* variables

	SPEI-1	SPEI-3	SPEI-6	SPEI-9	SPEI-12
SVI	0.366	0.365	0.350	0.377	0.375
SWI	0.382	0.405	0.415	0.417	0.404
ESI	0.530	0.612	0.606	0.564	0.519
SI-1[a]	0.572	0.585	0.586	0.579	0.543
SI-2	0.525	0.543	0.548	0.544	0.514
SI-3	0.521	0.532	0.531	0.536	0.509
SI-4	0.617	**0.632**	0.626	0.623	0.584

The highest correlation coefficient value are shown in bold.
[a]The formation of SI-1, SI-2, SI-3, and SI-4 are shown in Table 1.

The synthesized remote sensing variables (SI1, SI2, SI3, and SI4) showed higher correlations with various time scales of SPEI than SVI, SWI, and ESI in most cases. The correlation coefficient values between SVI and SPEI were lower than other indices. The reason may be that the SVI include more information on biophysical responses to drought than that captured by *in situ* drought index. In addition, SVI may also be sensitive to a number of environmental phenomena (e.g., hail, plant disease, wildfire, pest infestation), which would degrade vegetation conditions and result in a similar vegetation index signal, as seen in areas experiencing drought stress.

Table 2 also reveals that SWI was slightly more concordant with SPEI than SVI. The reason is that SWI was calculated from the NDWI, which is known by its sensitivity to vegetation water content and by its correlation to soil moisture [37]. In general, the correlation coefficient values between ESI and various time scales of SPEI were higher than SVI and SWI (Table 2). This is because evapotranspiration is the main expenditure in the water budget of this region, and ESI can reflect the water budget balance condition and drought degree, and hence, it seems logical that ESI was relatively better correlated with SPEI.

The correlation coefficient values between all four synthesized indices and *in situ* SPEI were higher than the values of single remote sensing indices, which proved that the synthesized indices were more satisfactory than SVI, SWI, and ESI alone. Together, the synthesized index provided a diversity of information about the drought conditions. This is advantageous because a convergence from multiple indicators provides better confidence in emerging drought signal.

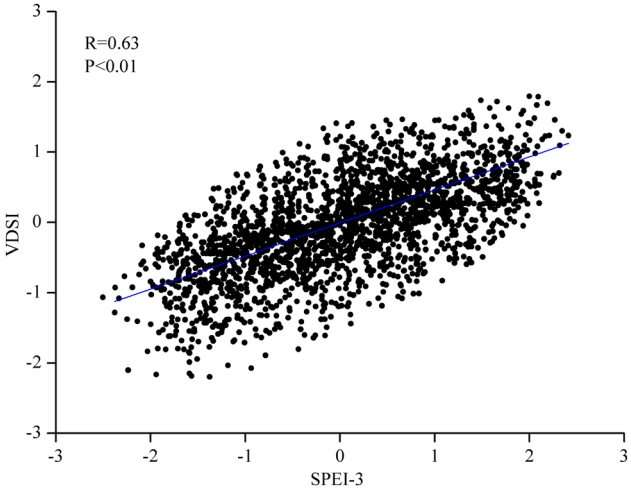

Figure 3: Scatter plot for VDSI and SPEI-3 from 2001 to 2010.

Table 3: Correlation between the VSDI and standardized variable of crop yield in growing period

	June	July	August	September
Soybean	0.27[a]	0.52[a]	0.49[a]	0.19[a]
Maize	0.22[a]	0.43[a]	0.41[a]	0.005

[a]Values significant at 0.01 probability level.

SI-4 performed better than other indices when correlated with SPEI (Table 2), and the correlation coefficient value was 0.632. As a result, SI-4 was selected as an optimum remote sensing drought index that outperformed other indices and was defined as VDSI. The performance of VDSI was examined by 1-, 3-, 6-, 9-, and 12-month SPEI, and the 3-month scale SPEI (SPEI-3) showed the highest correlation coefficient with VDSI. The scatter plot between VDSI and SPEI-3 is presented in Figure 3.

4.2 Validation using standardized variable of crop yield

A validation experiment was also carried out using the crop yield data. For the counties whose agriculture land area is more than 30% of the total area, correlation analyses were performed between the average VDSI value of the agriculture land and the county's crop yield anomaly. The results showed that the correlations between VDSI and the standardized variable of soybean and maize yields were significant for all cases except that between September VDSI value and maize yield (Table 3).

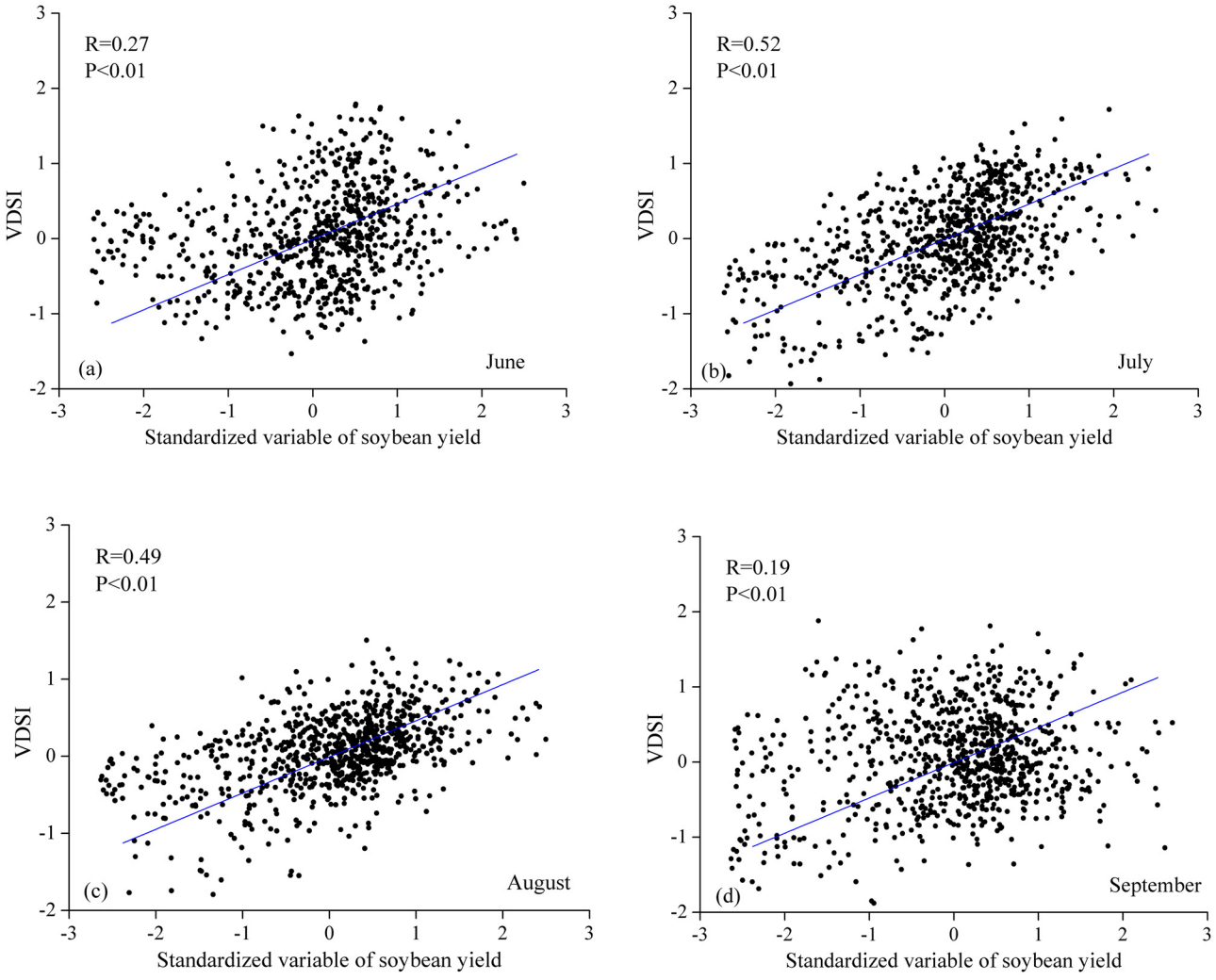

Figure 4: Scatter plots and correlation coefficient *R* values between VDSI and standardized variable of the soybean yield in soybean growing period (June–September) from 2001 to 2010.

The scatter plots between VDSI and standardized variable of soybean yield are shown in Figure 4. Each dot in the scatter plots showed yield versus VDSI for one county in the shown month. The spatial resolution of VDSI was 1 km at monthly time steps. The yearly yield data were collected at the county level. The results showed that VDSI of July had the highest correlation coefficient with soybean yield, followed by VDSI of August and June. The emergence stage of soybean is in June, and the pod setting stage of soybean is in July and August in the study area. Therefore, droughts occurred in these months are likely to result in a decrease of yield significantly.

The correlation coefficients between VDSI and maize yield variation were higher in July and August, when the maize was on the seeding stage. On the early vegetative stage of maize (June), the correlation between VDSI and maize yield variation was also significant at the 0.01 probability level. The correlation coefficient for June was lower than that for July and August. The reason may be that the seeding stage plays a more important role in yield formation. Maize is full seed and mature on September; therefore, the correlation coefficient between September VDSI and maize yield variation is very low and does not pass p value of <0.05 significant test (Figure 5).

These validations proved that VDSI can be used to monitor agricultural drought. However, the correlation coefficients between VDSI and the crop yield variation were not very high, which is partly because that the crop yield variation is not only influenced by drought but also by diseases, fertilization, and other natural disasters.

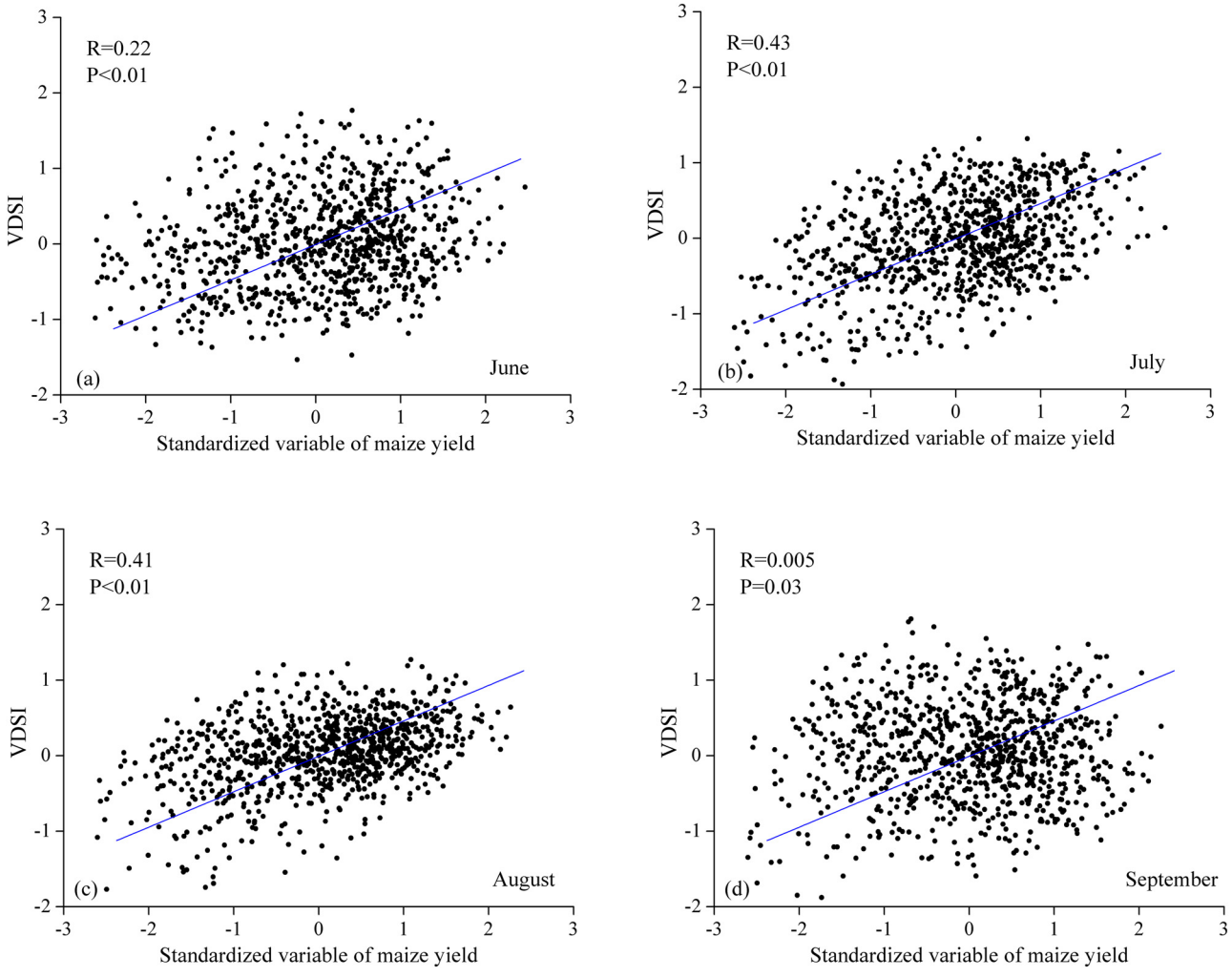

Figure 5: Scatter plots and correlation coefficient R values between VDSI and standardized variable of the maize yield in the maize growing period (June–September) from 2001 to 2010.

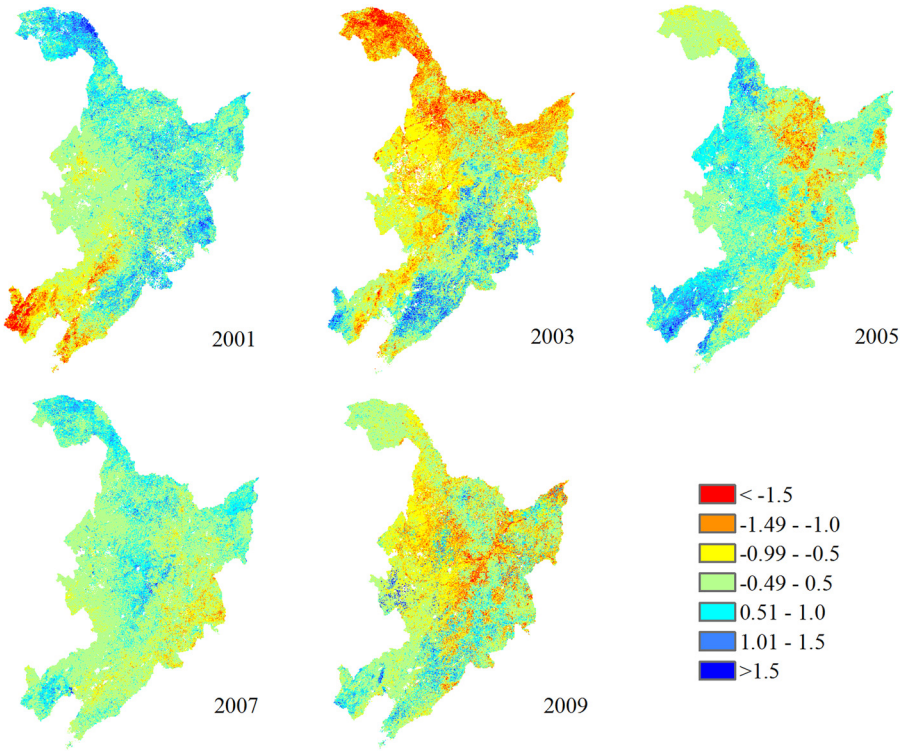

Figure 6: Spatial patterns of drought in northeast China monitored by VDSI for May every 2 years from 2001 to 2010.

4.3 Spatial-temporal drought process monitored by VSDI

In this region, rainfall is very low in the late spring (May), when drought disaster often happens [38]. July and August received more than 50% of the total precipitation. The drought conditions in the study area from 2001 to 2010 were monitored using the VSDI method in this research. The results showed that VSDI can reflect the severity and the extent of drought. The drought phenomenon detected by VDSI was in accordance with the historical observation in northeast China. For example, a serious dry period has been detected in northeastern China in May 2003. Most of the pasture and forest in the north and the agriculture land in the west of this region suffered drought in May 2003 [38]. In our research, the drought experienced in May 2003 was accurately monitored (Figure 6). Besides the drought

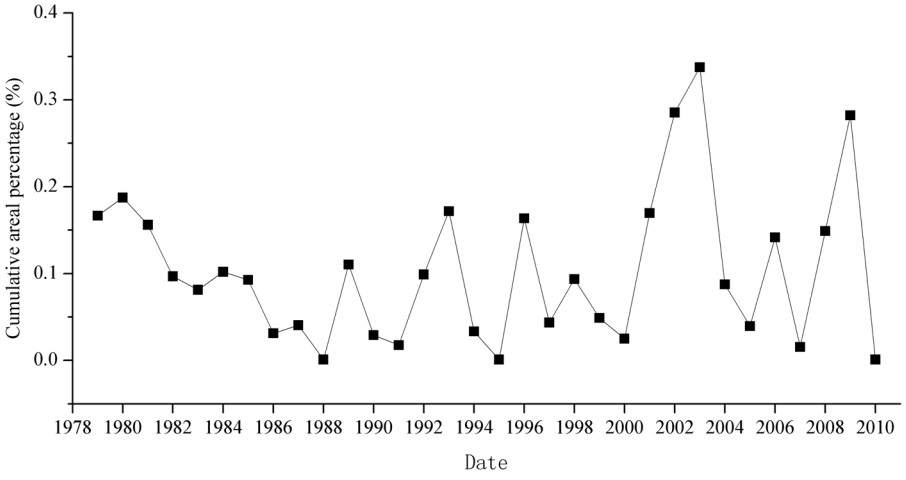

Figure 7: Cumulative percent area of the study area covered by dry condition (PDSI < −1) in May for 1979–2010.

happened in 2003, other droughts have also been monitored by VDSI, such as the drought occurred in 2009.

PDSI is commonly used to assess the performance of drought index. The PDSI data of the studied area from the study by Zhao et al. (2010) were analyzed [39]. Figure 7 shows the time series of cumulative percent area of the study area covered by the dry condition (PDSI < –1) for May from 1979 to 2010. We can see that larger area percent of this region was covered by drought in 2003 and 2009 than other years, which was in accordance with the results of this study (Figure 6).

4.4 Uncertainty analysis

The performance of VDSI may be improved by taking into account the following limitations: first, we cannot separate rained yield values. The yield data recorded the total crop production at the county level, and rained yield data are not available. In addition, we have no spatial distribution data for soybean and maize, and so the average VDSI value of the whole agriculture land was correlated with the yield data for each county. In the successive research, the rained yield values and the spatial distribution data for the main crops should be worked out, and based on this, the validation of the drought index through yield data would be more accurate. Second, we designed the synthesized drought index by weighing the percentage of each unique remote sensing data. The additive combination method was adopted because it is simple to use on large spatial scales. The precision may be improved if artificial intelligence (AI) models, genetic algorithm, and other advanced weighting methods are used to optimize the weight of each single drought index [40]. Third, the VDSI index was proved to be useful through comparing with the SPEI and crop yield data in this study. In the future, more indices should be taken into consideration in the validation, such as field measurement of soil moisture [41] and solar-induced chlorophyll fluorescence [42,43].

5 Conclusions

This study proposed a new synthesized drought index VDSI, which is the weighted combination of remote sensing drought indices of SVI, SWI, and ESI. Comparisons between the VDSI and *in situ* SPEI of several time scales were conducted over northeast China during 2001–2010 using the Pearson correlation analysis. The results showed that VDSI performed better than single remote sensing–based indices, and it showed a better correlation with SPEI-3 over the study area. Moreover, the variations of soybean and maize yields, which were standardized from the annual yields of each county, were used to do a correlation analysis with VDSI. The VDSI during growing seasons were well correlated with crop yield variations. These results proved that the new drought index integrating multisource vegetation response information can be used for drought monitoring in northeast China. The study is based on the freely available MODIS time series data, and the method is relatively simple to be carried out. Therefore, timely drought monitoring and mapping in large geographic areas can be achieved through the VDSI using the remote sensing data when there is a lack of the field measured data.

Acknowledgments: This research was funded by the National Key Research and Development Program of China (Grant No. 2018YFC1506605), National Natural Science Foundation of China (Grant No. 41501428 and 41371400), Natural Science Foundation of Shandong Province, China (Grant No. ZR2017BD010).

References

[1] Yu M, Li Q, Hayes MJ, Svoboda MD, Heim RR. Are droughts becoming more frequent or severe in china based on the standardized precipitation evapotranspiration index: 1951–2010? Int J Climatol. 2014;34:545–58.
[2] Wilhite DA, Glantz MH. Understanding the drought phenomenon: the role of definitions. Water Int. 1985;10:111–20.
[3] Dubovyk O, Ghazaryan G, Gonzalez J, Graw V, Loew F, Schreier J. Drought hazard in Kazakhstan in 2000–2016: a remote sensing perspective. Environ Monitor Assess. 2019;191:510.
[4] Liu X, Zhang J, Ma D, Bao Y, Tong Z, Liu X. Dynamic risk assessment of drought disaster for maize based on integrating multi-sources data in the region of the northwest of Liaoning Province, China. Nat Hazards. 2013;65:1393–409.
[5] FAOSTAT, Statistics database. Available at: http://faostat.fao.org/default.aspx (verified 25 May 2011), 2011.
[6] Chen Z, He X, Cook ER, He H-S, Chen W, Sun Y, et al. Detecting dryness and wetness signals from tree-rings in Shenyang, northeast China. Palaeogeograp Palaeoclimatol Palaeoecol. 2011;302:301–10.
[7] Yu X, He X, Zheng H, Guo R, Ren Z, Zhang D, et al. Spatial and temporal analysis of drought risk during the crop-growing season over northeast China. Nat Hazards. 2014;71:275–89.
[8] Vicente-Serrano SM, Beguería S, López-Moreno JI, Angulo M, El Kenawy A. A new global 0.5° gridded dataset (1901–2006)

of a multiscalar drought index: comparison with current drought index datasets based on the palmer drought severity index. J Hydrometeorol. 2010;11:1033–43.
[9] Zhao N, Yue T, Li H, Zhang L, Yin X, Liu Y. Spatio-temporal changes in precipitation over Beijing–Tianjin–Hebei region, China. Atmos Res. 2018;202:156–68.
[10] Rojas O, Vrieling A, Rembold F. Assessing drought probability for agricultural areas in africa with coarse resolution remote sensing imagery. Remote Sens Environ. 2011;115:343–52.
[11] Zargar A, Sadiq R, Naser B, Khan FI. A review of drought indices. Environ Rev. 2011;19:333–49.
[12] Song X, Li L, Fu G, Li J, Zhang A, Liu W, et al. Spatial-temporal variations of spring drought based on spring-composite index values for the Songnen plain, northeast China. Theor Appl Climatol. 2014;116:371–84.
[13] Du L, Tian Q, Yu T, Meng Q, Jancso T, Udvardy P, et al. A comprehensive drought monitoring method integrating modis and trmm data. Int J Appl Earth Observ Geoinform. 2013;23:245–53.
[14] Garcia M, Fernández N, Villagarcía L, Domingo F, Puigdefábregas J, Sandholt I. Accuracy of the temperature-vegetation dryness index using modis under water-limited vs. energy-limited evapotranspiration conditions. Remote Sens Environ. 2014;149:100–17.
[15] Bhattarai N, Quackenbush LJ, Dougherty M, Marzen LJ. A simple landsat-modis fusion approach for monitoring seasonal evapotranspiration at 30 m spatial resolution. Int J Remote Sens. 2015;36:115–43.
[16] Kogan F. Application of vegetation index and brightness temperature for drought detection. Adv Space Res. 1995;15:91–100.
[17] Peters AJ, Waltershea EA, Hayes M, Svoboda MD. Drought monitoring with ndvi-based standardized vegetation index. Am Soc Photogram Remote Sens. 2002;68:71–5.
[18] Gao BC. NDVI-a normalized difference water index for remote sensing of vegetation liquid water from space. Remote Sens Environ. 1996;58:257–66.
[19] Anderson MC, Hain C, Wardlow B, Pimstein A, Mecikalski JR, Kustas WP. Evaluation of drought indices based on thermal remote sensing of evapotranspiration over the continental united states. J Clim. 2011;24:2025–44.
[20] Han H, Bai J, Yan J, Yang H, Ma G. A combined drought monitoring index based on multi-sensor remote sensing data and machine learning. Geocarto Int. 2019. doi: 10.1080/10106049.2019.1633423.
[21] Choi M, Jacobs JM, Anderson MC, Bosch DD. Evaluation of drought indices via remotely sensed data with hydrological variables. J Hydrol. 2013;476:265–73.
[22] Rhee J, Im J, Carbone GJ. Monitoring agricultural drought for arid and humid regions using multi-sensor remote sensing data. Remote Sens Environ. 2010;114:2875–87.
[23] Zhang A, Jia G. Monitoring meteorological drought in semiarid regions using multi-sensor microwave remote sensing data. Remote Sens Environ. 2013;134:12–23.
[24] Hao C, Zhang J, Yao F. Combination of multi-sensor remote sensing data for drought monitoring over southwest China. Int J Appl Earth Observ Geoinform. 2015;35:270–83.
[25] Brown JF, Wardlow BD, Tadesse T, Hayes MJ, Reed BC. The vegetation drought response index (VegDRI): a new integrated approach for monitoring drought stress in vegetation. GIScience Remote Sens. 2008;45:16–46.
[26] Wang Z, Schaaf CB, Sun Q, Shuai Y, Román MO. Capturing rapid land surface dynamics with collection v006 MODIS BRDF/NBAR/Albedo (MCD43) products. Remote Sens Environ. 2018;207:50–64.
[27] Wang M, Tao F, Shi W. Corn yield forecasting in northeast china using remotely sensed spectral indices and crop phenology metrics. J Integr Agric. 2014;13:1538–45.
[28] Schaaf CB, Gao F, Strahler AH, Lucht W, Li X, Tsang T, et al. First operational BRDF, Albedo Nadir reflectance products from MODIS. Remote Sens Environ. 2002;83:135–48.
[29] Peng J, Liu Q, Wen J, Liu Q, Tang Y, Wang L, et al. Multi-scale validation strategy for satellite albedo products and its uncertainty analysis. Sci China (Earth Sci). 2015;573–88.
[30] Mu Q, Zhao M, Kimball JS, McDowell NG, Running SW. A remotely sensed global terrestrial drought severity index. Bull Am Meteorol Soc. 2012;94:83–98.
[31] Wang H, Lin H, Liu D. Remotely sensed drought index and its responses to meteorological drought in southwest China. Remote Sens Lett. 2014;413–22.
[32] Liu J, Kuang W, Zhang Z, Xu X, Qin Y, Ning J, et al. Spatiotemporal characteristics, patterns, and causes of land-use changes in china since the late 1980s. J Geograph Sci. 2014;24:195–210.
[33] Anderson MC, Hain C, Wardlow B, Pimstein A, Mecikalski JR, Kustas WP. Evaluation of drought indices based on thermal remote sensing of evapotranspiration over the continental united states. J Clim. 2010;24:2025–44.
[34] Kogan FN. Global drought watch from space. Bull Am Meteorol Soc. 1997;78:621–36.
[35] Patel N, Yadav K. Monitoring spatio-temporal pattern of drought stress using integrated drought index over Bundelkhand region, India. Nat Hazards. 2015;77:663–77.
[36] Vicente-Serrano SM, Beguería S, López-Moreno JI. A multiscalar drought index sensitive to global warming: the standardized precipitation evapotranspiration index. J Clim. 2009;23:1696–718.
[37] Ezzine H, Bouziane A, Ouazar D. Seasonal comparisons of meteorological and agricultural drought indices in morocco using open short time-series data. Int J Appl Earth Observ Geoinform. 2014;26:36–48.
[38] Zeng LH, Song KS, Zhang B. Spatial and temporal structure of water deficitover northeast China during the period of 1951–2008. J Nat Res. 2011;26:858–70.
[39] Zhao M, Running SW. Drought-induced reduction in global terrestrial net primary production from 2000 through 2009. Science. 2010;329:940–3.
[40] Alizadeh MR, Nikoo MR. A fusion-based methodology for meteorological drought estimation using remote sensing data. Remote Sens Environ. 2018;211:229–47.
[41] Cong D, Zhao S, Chen C, Duan Z. Characterization of droughts during 2001–2014 based on remote sensing: a case study of northeast China. Ecol Inform. 2017;39:56–67.
[42] Chen X, Mo X, Zhang Y, Sun Z, Liu Y, Hu S, et al. Drought detection and assessment with solar-induced chlorophyll fluorescence in summer maize growth period over north china plain. Ecol Indic. 2019;104:347–56.
[43] Hu M, Kimball JS, Yi Y, Running S, Guan K, Jensco K, et al. Impacts of the 2017 flash drought in the us northern plains informed by satellite-based evapotranspiration and solar-induced fluorescence. Environ Res Lett. 2019;14:074019.